PROCEEDINGS, 51st Workshop on Geothermal Reservoir Engineering
Stanford University, Stanford, California, February 9-11, 2026
SGP-TR-230

Characterizing the geothermal potential at Lund North, UT using 2D and 3D geophysical and geologic models

Grant H. Rea-Downing[1*], Jonathan M. Glen[1], Jared Peacock[1], Jeff Witter[2], Christian Hardwick[3], Eugene Szymanski[3], Stephan Kirby[3], Nicole Hart-Wagoner[4], and James Faulds[4]

[1]U.S. Geological Survey, Moffett Field, CA 94035

[2]Innovate Geothermal, Vancouver, BC Canada

[3]Utah Geological Survey, Salt Lake City, UT 84116

[4]Great Basin Center for Geothermal Energy, Nevada Bureau of Mines and Geology, University of Nevada, Reno, NV 89557

*grea-downing@usgs.gov

Keywords: INGENIOUS, geophysics, geology, forward modeling, 3D modeling, gravity, magnetics, magnetotellurics

ABSTRACT

The INovative Geothermal Exploration through Novel Investigations Of Undiscovered Systems (INGENIOUS) project is a United States Department of Energy-funded multi-year project which seeks to identify and characterize blind geothermal systems in the Great Basin region. Geothermal systems in this region are predominantly fault-controlled geothermal plays and most reside in favorable structural settings (e.g. fault intersections, stepovers, etc.). Lund North, UT is the fourth detailed study site selected for the INGENIOUS project and is located along a complex fault-bend and stepover zone of the Lund fault in the southernmost Wah Wah Mountains of Iron County, Utah. Here we present new 2D and 3D modeling results derived from a broad range of geophysical data collected at the Lund North site including airborne magnetic data, ground-based gravity and magnetotelluric (MT) data, paleomagnetic (remanence) directional data, and magnetic susceptibility and density data obtained from hand samples collected in the field. Together these were used in conjunction with existing 1:50,000 scale geologic maps and a 2D seismic line to construct six 2D forward geophysical models across the study region which constrain the subsurface geology and inform potential drilling targets. These six forward models serve as the primary inputs for a 3D geologic model of the Lund North site which further improves our understanding of the subsurface and highlights the structural complexity of the site as well as the relationship between mapped and inferred structures and the 3D resistivity model derived from MT data. Surfaces from the 3D geologic model will be used as constraints for 3D inversion of the gravity and magnetic data collected at Lund North to improve model consistency with the observations and ultimately to inform selection of drilling targets for thermal gradient wells.

1. INTRODUCTION

The INGENIOUS project, which focuses on exploration of blind geothermal systems that lack clear surface expression, relies on integrating a diverse set of geologic and geophysical data to infer geothermal favorability of sites throughout much of the Great Basin (Ayling et al., 2022). The project scope is two-fold: (1) combine previous Play Fairway Analysis approaches with conceptual and 3D modeling and machine learning techniques to create regional geothermal favorability maps of the Great Basin as primary tools for geothermal exploration, and (2) use these regional maps and models to explore several prospective local sites in greater detail utilizing new and existing data to construct detailed 3D models for use in thermal gradient hole site selection. The project has chosen four such sites including Granite Springs Valley (e.g., Faulds et al., 2019; Glen et al., 2022), Argenta Rise (e.g., Earney et al., 2024; Faulds et al., 2024), and Buffalo Valley (Burgess & Faulds, 2024) in Nevada and the Lund North site in southwest Utah (Hardwick et al., 2025). Each of these sites were chosen based on the regional favorability models constructed for the Nevada Play Fairway Analysis Project (e.g., Faulds et al., 2021) and the INGENIOUS project (Hart-Wagoner et al., 2024) and their favorable structural settings (Faulds & Hinz 2015).

Additional field work and data collection were conducted at each local study site to complement existing data and improve the resolution of resulting models. Data collection included 2-meter temperature surveys, fluid geochemical analysis, updated structural mapping, gravity station collection, outcrop magnetic susceptibility measurements, and magnetotelluric (MT) surveys. Physical sampling included rock samples for density and magnetic susceptibility measurements as well as oriented paleomagnetic samples to constrain magnetic remanence in 2D and 3D geophysical modeling. Here, we present results from the Lund North site which benefitted from the recently acquired aeromagnetic data collected as part of the U.S. Geological Survey (USGS) Earth Mapping Resource Initiative (Earth MRI) project (Day, 2019). The Lund North site sits at the southern margin of the recently published west central Utah airborne magnetic survey (Schermerhorn & Phelps, 2025). The site also includes a previously collected 2D seismic line.

We present a geophysical analysis of the Lund North site including 2D models constructed using newly collected gravity and aeromagnetic data. The models are constrained by density and magnetic susceptibility data collected from 24 outcrops along with paleomagnetic samples and outcrop magnetic susceptibility readings collected from six sites to constrain magnetic susceptibility and remanence in the 2D models. These models serve as inputs along with existing 1:50,000 scale geologic mapping and updated lidar-based fault mapping to construct a 3D geologic model of the site. This model is combined with a 3D resistivity model constructed from the MT survey to help identify areas of interest for thermal gradient well sites.

2. GEOLOGIC SETTING

Lund North is situated in the southwest corner of the Great Basin in the Escalante Desert approximately 50 kilometers northwest of Cedar City, UT (Figure 1). The site sits at the southernmost end of the Wah Wah Mountains which expose Oligocene-Miocene volcanics in the footwall of the Lund fault (Hintze et al., 1994) and demarcates the range front. Geologic mapping by Hintze et al. (1994) indicates that, locally, the volcanic packages sit atop a thin deposit of Eocene-age Claron Formation, a conglomeratic quartzite which unconformably overlies the Jurassic Navajo Sandstone of the Glen Canyon Group. The Mesozoic stratigraphy sits upon and is (in places outside our field area) overthrust by Paleozoic stratigraphy consisting primarily of carbonates and shales. In addition to the active range front fault, the range contains a series of older, presumed inactive normal faults which dissect the range and expose various portions of the stratigraphy. Prominent volcanic units include the extensive Isom and Lund Formations which together with the Wah Wah Springs and Escalante Desert Formations represent voluminous Oligocene-age volcanic activity associated with the Indian Peak-Caliente Caldera system to the west (Best et al., 2013). These dense welded tuffs sit above a mix of thinner tuffs and volcanic breccias and are overlain by Miocene-age bimodal volcanic rocks associated with more modern basin and range volcanism. The basin is characterized by typical Basin and Range Quaternary alluvial, colluvial, and lacustrine deposits with the northern portion of the study site resting primarily on the southern flank of a large alluvial fan which drains the range to the northwest.

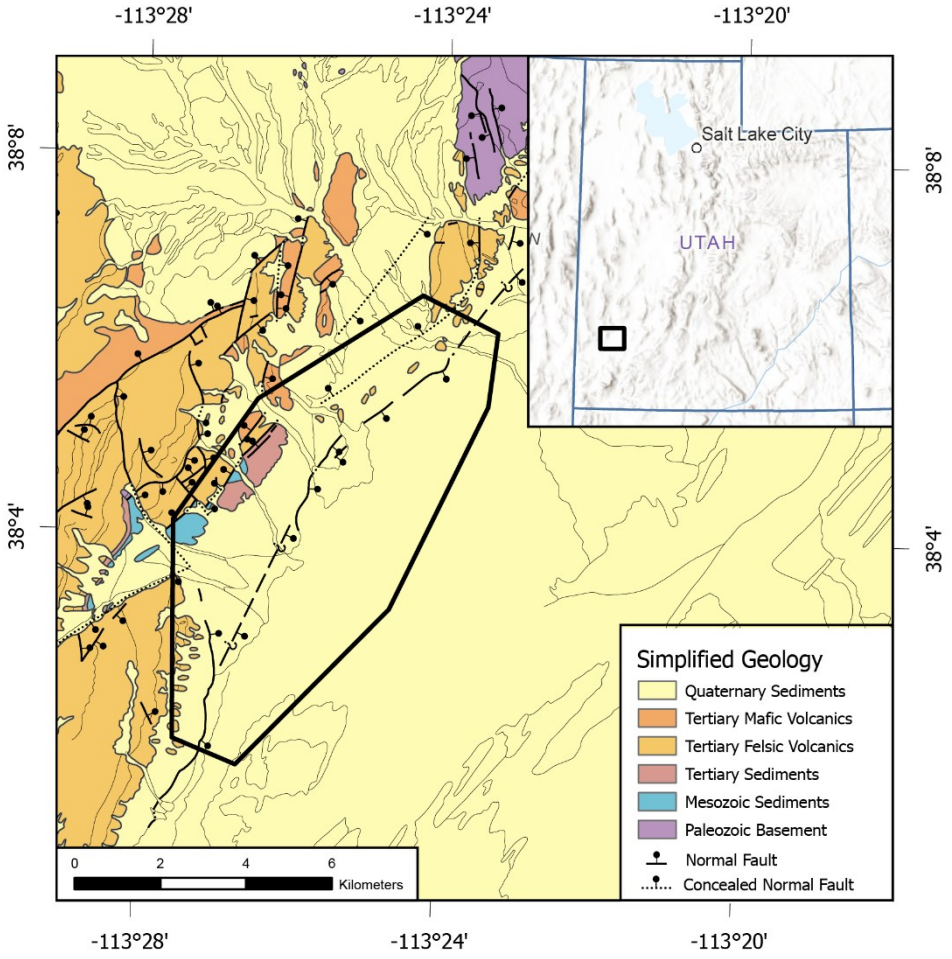

Figure 1: Map showing the Lund North field site (black polygon) as well as the local geology simplified from the mapping of Hintze et al. (1994, 2017). Inset regional map data from the U.S. Geological Survey's National Map Dataset showing the location of the study area in southwest Utah (black box).

3. METHODS & DATA

3.1 Gravity

A total of 241 new gravity stations were collected to improve regional coverage in and around Lund North. Data were collected by the Utah Geological Survey in the spring of 2024 using Scintrex CG-5 model gravity meters (Scintrex Ltd, Concord, CA-ON) following collection and processing methods outlined in Gettings et al. (2008). These data were reprocessed by the USGS along with ~400 regional gravity stations to include lidar-based terrain corrections and then assessed for quality and consistency throughout the Lund North field site. Regional data are from the Pan American Center for Earth and Environmental Studies (PACES) dataset (Hildenbrand et al., 2002) made available from University of Texas, El Paso on 5/29/2018 (Ben Denth, U.S. Geological Survey, written comm., March 2021). The

newly collected data substantially improve gravity station coverage in the Lund North area with several detailed lines collected across major structures at 100- to 300-m station spacing to ensure any geophysical manifestation of the range front faults were well characterized. Isostatic anomaly values were calculated for each station following standard reduction methods (Blakely, 1995) wherein an average crustal density of 2,670 kg/m^3 is assumed along with a 25-km crustal thickness and a crust-mantle density contrast of 400 kg/m^3. From these data, we construct an isostatic anomaly grid with a cell size of 200 m across the Lund North field site (Figure 2). We then compute the horizontal gradient magnitude of the isostatic anomaly (as described in Blakely & Simpson, 1986) from which we derive lineations of horizontal gradient maxima that allow us to identify geophysical lineaments that represent substantial lateral changes in density (Cronkite-Ratcliff & Athens, 2025). These features which commonly occur along faults or contacts are shown overlain on the isostatic anomaly grid in Figure 2 and serve as important constraints for detection and location of structures and contacts that may not have clear surface expression. These maxima augment the updated lidar-based structural mapping conducted by the Utah Geological Survey as part of this project (see section 3.4).

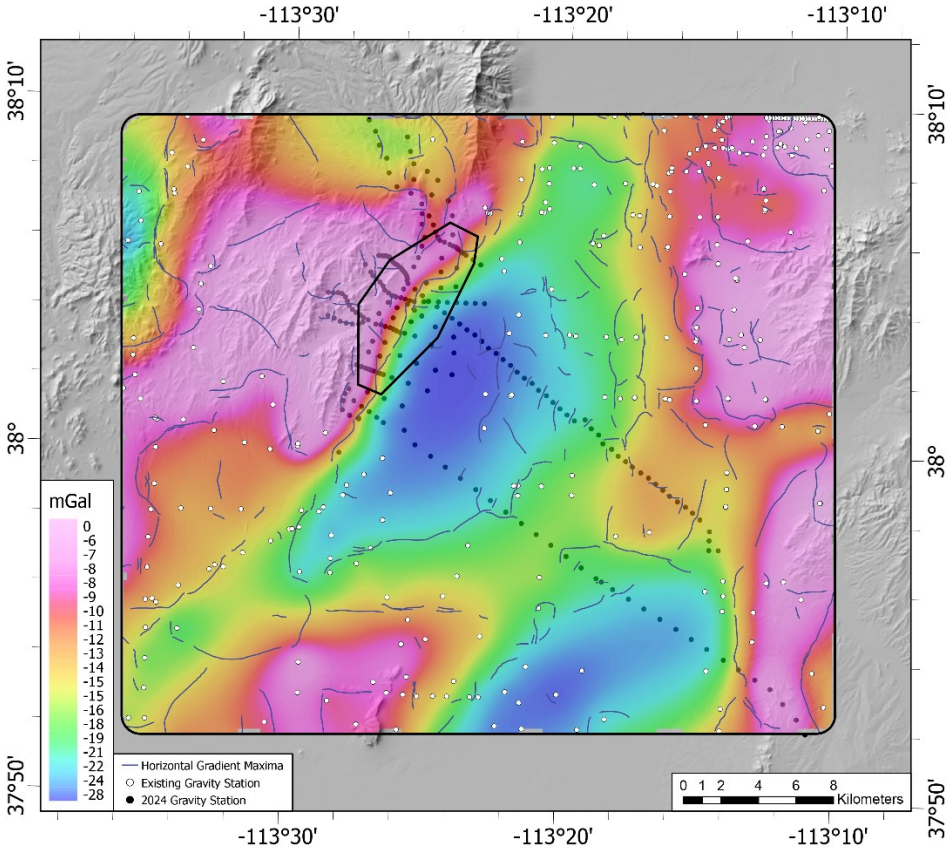

Figure 2: Topographic hillshade of the broader Lund North field area overlain by the isostatic gravity anomaly computed from existing (white) and new (black) gravity stations collected in the Lund North area. The study area is represented by the black polygon. Blue lines represent locations of maximum horizontal gradient computed from the isostatic anomaly grid. The topographic hillshade was generated from a 30-m digital elevation model (DEM) taken from the U.S. Geological Survey National Map (U.S. Geological Survey, 2024).

3.1.1 Depth to Basement

We use the updated gravity data collected here to conduct a 3D inversion of gravity anomalies in the Lund North region to estimate the depth to basement in the field site. The method, described in detail by Jachens & Morring (1990), is constrained by gravity measurements and a simplified geologic map that classifies all units into one of two categories: 1) basement (generally any crystalline units or pre-Cenozoic age formations) or 2) basin fill. Gravity measurements collected on basement are used to calculate a basement gravity field (the component of gravity anomalies deriving from basement). The basement gravity field is then subtracted from the observed gravity anomaly (which incorporates both basement and basin gravity measurements) to produce a basin gravity field that is subsequently used to estimate depth to basement. The inversion maintains a static density depth function for basin fill and iteratively adjusts the depth of the basement surface beneath basin fill, while attempting to reproduce the basin gravity field, until changes between iterations are minimal. The inversion is highly dependent on the quality and quantity of gravity stations collected on basement as well as the density function chosen for basin fill (we follow the density function outlined in Jachens et al., 1996). The choice of what constitutes "basement" geology can be challenging with respect to volcanic units present throughout the Basin and Range – generally volcanic units represent a "middle ground" between low density basin sediments and older crystalline units and can be classified as either. In our case at Lund North, we chose to classify them as basement given that where they are mapped locally in the range the volcanic units are thick welded tuffs more likely to approximate basement. In addition, the basement gravity station coverage is still somewhat sparse at the Lund North site, so the results of

the inversion are likely relatively imprecise. Nevertheless, Figure 3 shows the result of the inversion for the Lund North region and suggests a ~1.5-km deep basin immediately southeast of the Lund North site.

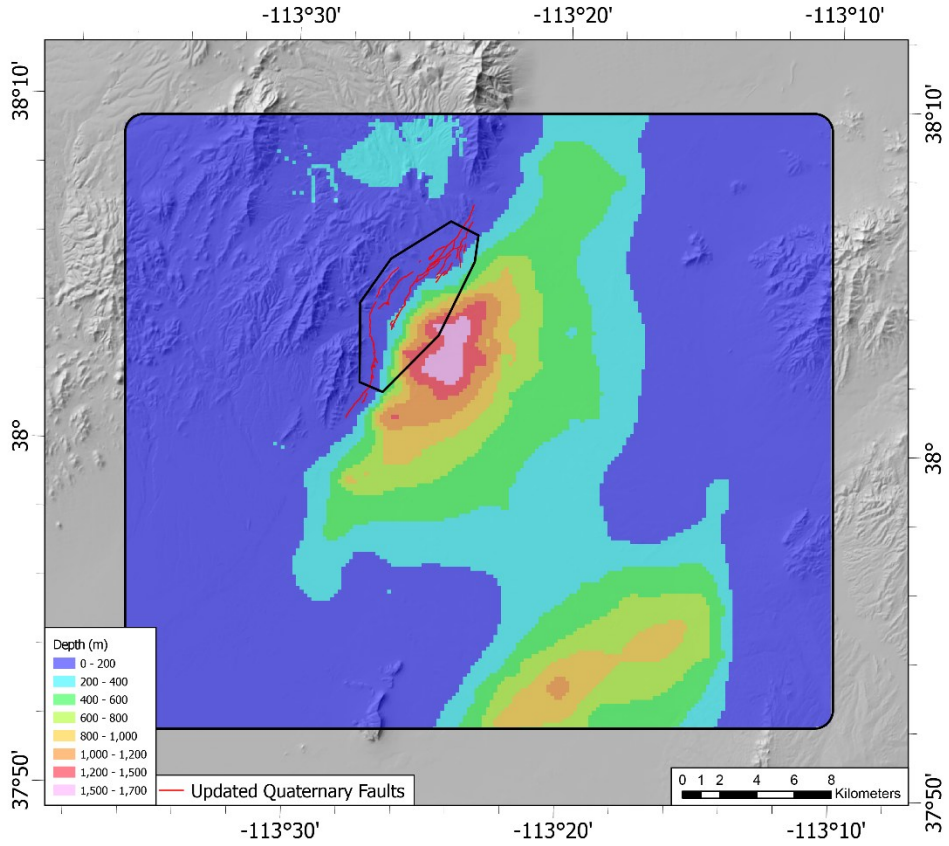

Figure 3: Depth to basement inversion results based on the new and legacy gravity data in the Lund North region. The study area boundary is represented by the black polygon. Red lines represent updated Quaternary fault mapping conducted by the Utah Geological Survey as part of this project (see section 3.4). The topographic hillshade was generated from a 30-m DEM taken from the U.S. Geological Survey National Map (U.S. Geological Survey, 2024).

3.2 Magnetics

3.2.1 Aeromagnetic Survey

Aeromagnetic data were collected over a large portion of west central Utah between August 2023 and October 2024 as part of the USGS Earth MRI program (see Day, 2019). Data were collected on a combination of fixed wing and helicopter aircraft at a nominal height of 100 m above ground level with 200-m line spacing. Additional details of the survey design as well as data processing steps are outlined in the public data release associated with the survey (Schermerhorn & Phelps, 2025). A second survey was flown soon after the first that adjoins the west central Utah survey and covers the southern portion of the Lund North field site. At the time of publication, these data were not publicly available (USGS, EarthMRI). It was flown by the same contractors and includes identical survey parameters and data processing methods as the west central Utah survey. Together these two surveys cover the entire Lund North field site and allow us to construct a high-resolution magnetic anomaly map of the site (Figure 4). We use the magnetic map to create lineations representing horizontal gradient maxima following a process similar to what was outlined for the gravity data in section 3.1. A pseudogravity transformation is performed on the total field magnetic data prior to calculation of the horizontal gradient magnitude (Blakely & Simpson, 1986). This transformation shifts magnetic anomalies to be centered over their sources and, as with the gravity data, allows for mapping of lateral contrasts in magnetic properties throughout the Lund North field area.

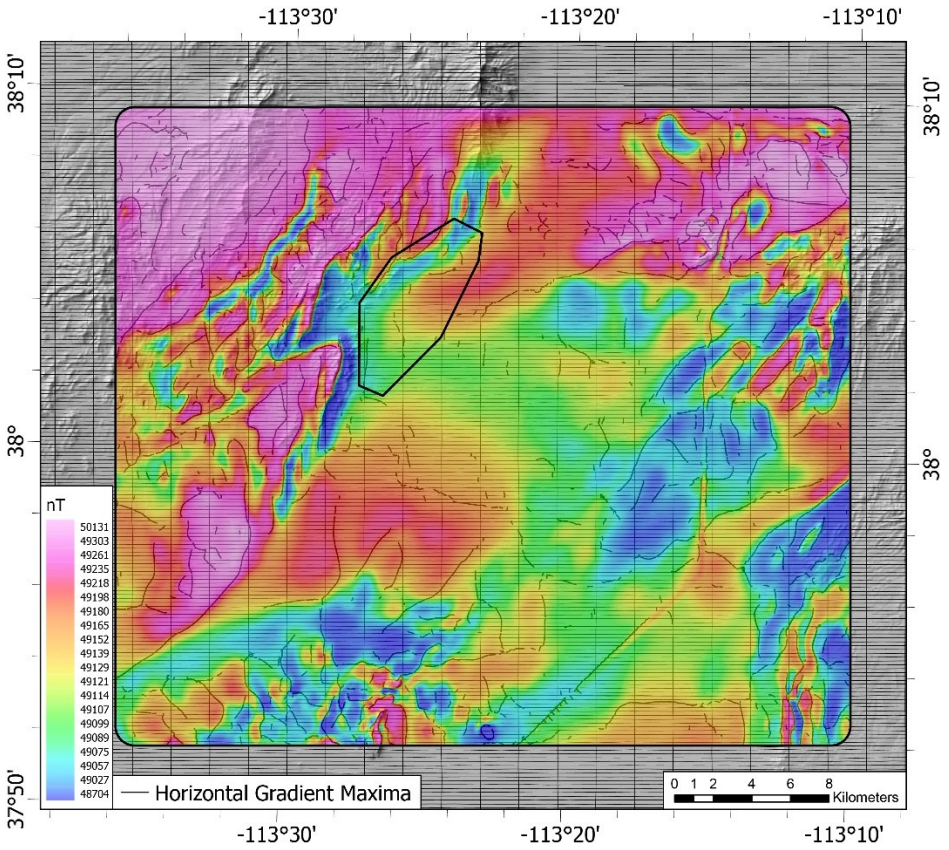

Figure 4: Topographic hillshade of the broader Lund North field area overlain by the reduced-to-pole magnetic anomaly grid computed from aeromagnetic surveys conducted over the Lund North site. The study area boundary is represented by the black polygon. Bold black lines are lines of maximum horizontal gradient computed from the magnetic grid. The topographic hillshade was generated from a 30-m DEM taken from the U.S. Geological Survey National Map (U.S. Geological Survey, 2024).

3.2.2 Paleomagnetic Data

In addition to the aeromagnetic data described above we collected oriented paleomagnetic cores from multiple volcanic units throughout the Lund North field area to constrain the effect of magnetic remanence in the aeromagnetic data. We targeted the most extensive and voluminous units to maximize the utility of the data during modeling and collected samples at six sites throughout the field area comprising 49 individual cores. Samples were collected with a gas-powered, water-cooled rock drill and oriented using a magnetic compass in a Pomeroy orienter (ASC Scientific, Narragansett, RI) along with sun compass measurements when possible. Measurements were conducted at the Utah Paleomagnetic Center at the University of Utah. Samples were stepwise demagnetized in an alternating field and measured after each step using an Agico JR-6 spinner magnetometer (AGICO, Brno, Czech Republic). Directions were fit primarily using principal component analysis or great circle fits where necessary. Table 1 lists the resultant site-mean directions for each of the sampled locations in the field area. Site locations are shown in Figure 5 which also includes an updated map of the geology that separates units based on their magnetic polarity as recorded in the paleomagnetic data. The presence of the reversed units is clearly indicated in the aeromagnetic data (especially the reversed Wah Wah Springs Formation) suggesting that magnetic remanence is exerting a primary control over the magnetic character of the geology at the Lund North site.

Table 1: Site mean directions from the six sampled volcanic units in the field area along with the magnetic polarity assumed for the unit in subsequent modeling. All geologic units are part of the Needles Range Group except for the Isom and Blawn Formations.

Geologic Unit	Site Mean Declination (°)	Site Mean Inclination (°)	Magnetization (A/m)	Polarity (R/N)	Figure 5 Map Pattern
Lamerdorf Tuff Member of the Escalante Desert Formation	221.6	-34.6	0.07	R	

Andesite member of the Escalante Desert Formation	187.5	-55	0.03	R	
Wah Wah Springs Formation	197.2	-49	1.61	R	
Lund Formation	31.5	51.9	3.34	N	
Isom Formation	201.6	-47.5	0.1	R	
Blawn Formation	332.6	68.4	0.58	N	

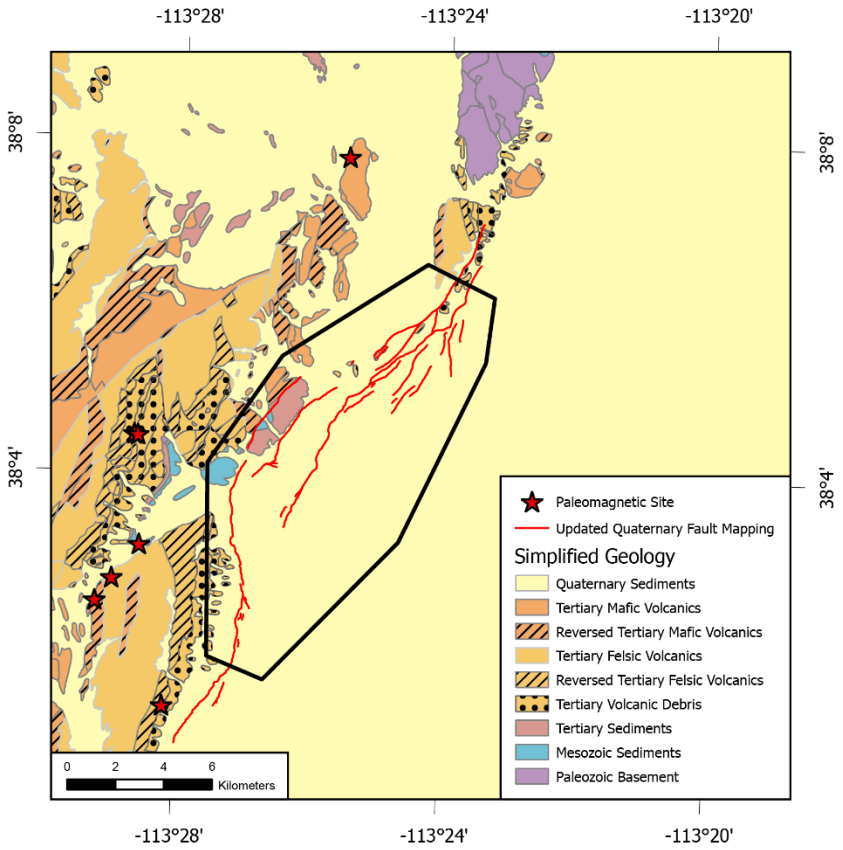

Figure 5: Simplified geologic map of the Lund North field site showing the paleomagnetic sampling locations described above. The geology, simplified from Hintze et al. (1994), has been updated to reflect the magnetic polarity of the volcanic units exposed in the area. Updated Quaternary faults are shown in red (see section 3.4). The study area boundary is represented by the black polygon.

3.3 Magnetotellurics

In May of 2024, magnetotelluric (MT) data were obtained from 52 stations spread throughout the Lund North site (Figure 6). The details of the instrumentation as well as data processing are outlined in Hardwick et al. (2025) and follow workflows described in Peacock et al. (2022, 2024) and Kapler et al. (2024). The processed data were used to construct a 3D resistivity model using the inversion software ModEM (Kelbert et al., 2014) to identify regions of potential hydrothermal activity and/or the presence of fluids and alteration in the subsurface. Breaks in conductivity can be caused by subsurface structure and can help constrain faults at depth. Cross sections of the model are extracted along the 2D models described in section 3.5 to augment subsurface interpretations. Given that the strength of the

MT data is in their inherent 3D nature, we integrate the resistivity model with the 3D geologic model described in section 3.6 to help elucidate the relationship between mapped and modeled structures and low resistivity anomalies in the subsurface at Lund North.

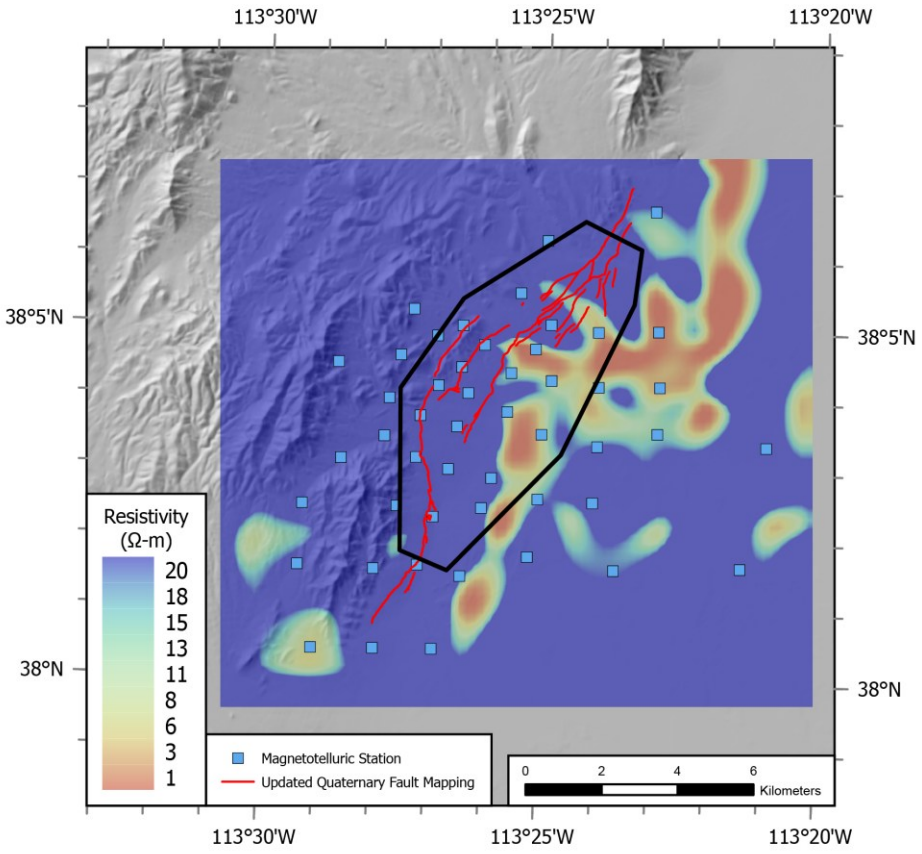

Figure 6: Map showing the location of magnetotelluric stations collected throughout the Lund North field area in the spring of 2024. Also shown is a 1000-m depth slice taken from the 3D resistivity model developed from the data which highlights the most conductive anomalies (<20 Ohm-m) in the region. Updated Quaternary faults shown in red. The study area is represented by the black polygon. The topographic hillshade was generated from a 30-m DEM taken from the U.S. Geological Survey National Map (U.S. Geological Survey, 2024).

3.4 Structural Mapping

In the spring of 2024, the Utah Geological Survey collected ~10.15 km^2 of new high resolution lidar data using an uncrewed aerial system (UAS). A DJI Matrice M300 UAS with a DJI Zenmuse L1 lidar scanner (DJI, Shenzhen, China) was used for data collection. Details of the data collection and processing are outlined in Hardwick et al. (2025). The resulting DEM has a 0.22 m/pixel resolution and allows for high-resolution mapping of Quaternary-age fault scarps (Figure 7). The new DEM was used in conjunction with 1-m resolution lidar data already available in the area (UGRC, 2020) to update the Quaternary fault mapping of the entire Lund North field site. The resulting fault map is combined with faults found on the geologic map of Hintze et al. (1994) for use in the 2D and 3D modeling effort.

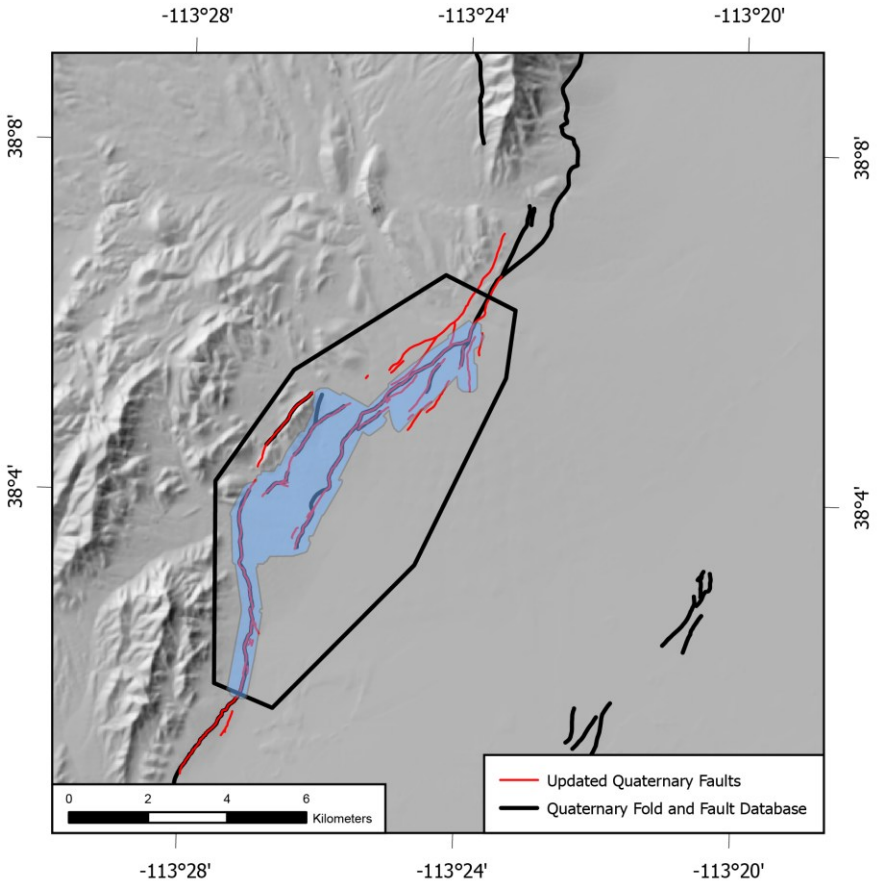

Figure 7: Shaded relief map of the Lund North study site showing the new UAS lidar data collected by the Utah Geological Survey in red compared with the U.S. Geological Survey Quaternary Fault and Fold Database (U.S. Geological Survey, 2020) in black. UAS data collection area is shown by the blue polygon. The study area is represented by the black polygon. The topographic hillshade was generated from a 30-m DEM taken from the U.S. Geological Survey National Map (U.S. Geological Survey, 2024).

3.5 2D Geophysical Modeling

Six profile lines were chosen to construct 2D geophysical models of the Lund North site. Five lines were drawn roughly perpendicular to structural trends and in areas with the best gravity station coverage. A single crossing profile was chosen to help tie the other sections together for better integration with the 3D geologic model described below. Figure 8 shows the location of each profile line as well as the location of samples taken for physical rock property measurements (magnetic susceptibility and density). The rock property and paleomagnetic data were used to redefine existing geologic maps (Hintze et al., 1994, 2017) into the simplified stratigraphy used in both the 2D and 3D models. Model units were delineated by lithology (sedimentary vs volcanic), age, and variations in their rock properties. Final values of rock properties for each model unit are listed in Table 2.

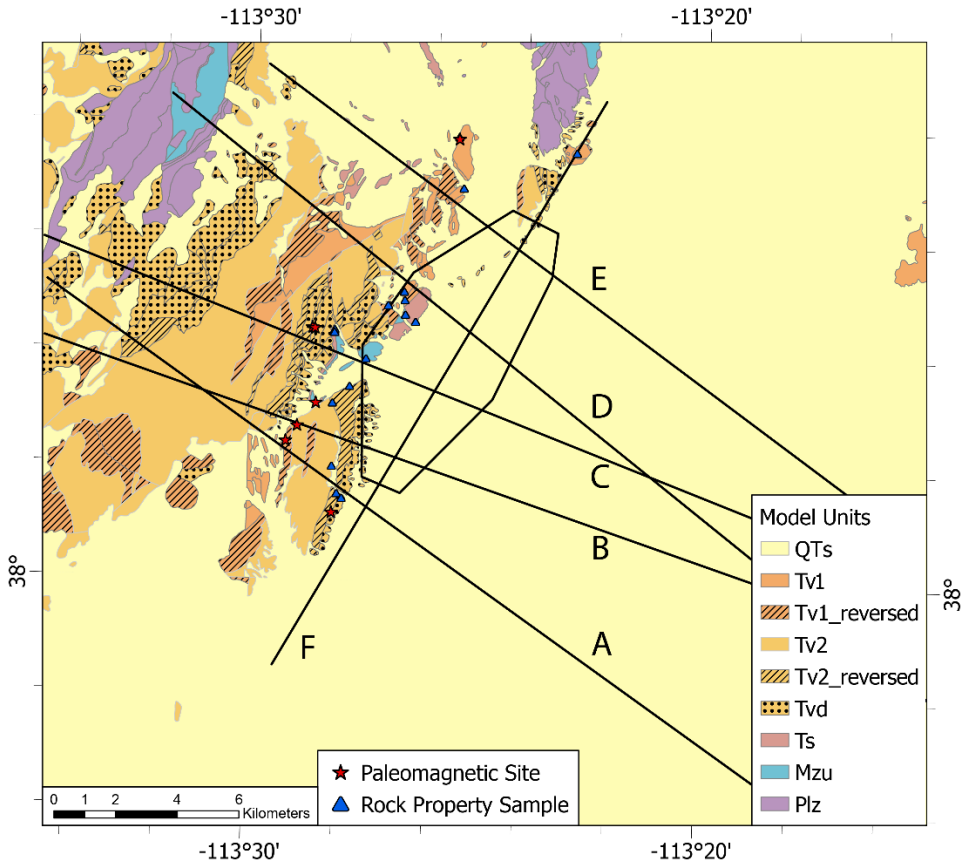

Figure 8: Simplified geologic map showing the 2D model profiles labeled A-F along with rock property sample locations (blue triangles), paleomagnetic sites (red stars), and the model units as defined in Table 2. The study area boundary is represented by the black polygon.

Table 2: Physical rock property values used in 2D profile modeling including density, magnetic susceptibility, magnetic inclination and declination, and magnetization.

Model Unit	Description	Density (kg/m^3)	Magnetic Susceptibility (SI)	Site Mean Declination (°)	Site Mean Inclination (°)	Magnetization (A/m)
QTs	Quaternary sediments	2,200	0	0	0	0
Tv1	Tertiary mafic volcanics	2,402	0.009	332.6	68.4	0.577
Tv1_reversed	Reversed Tertiary mafic volcanics	2,530	0.009	201.6	-47.5	0.104
Tv2	Tertiary felsic volcanics	2,594	0.003	31.5	51.9	3.34
Tv2_reversed	Reversed Tertiary felsic volcanics	2,555	0.001	197.2	-49.0	1.61
Tvd	Tertiary volcanic debris	2,416	0.001	207.7	-46.0	0.046
Ts	Tertiary sediments	2,614	0	0	0	0
Mzu	Mesozoic sediments	2,579	0	0	0	0
Pzl	Paleozoic Basement	2,730	0	0	0	0

We constructed six 2D models using the Oasis Montaj GM-SYS 2D modeling software extension (Seequent, 2024) which allows joint forward modeling of gravity and magnetic data. Each 2D profile is consistent with the simplified geologic map at the surface and uses an interpreted 2D seismic profile and the depth to basement surface to help constrain subsurface contacts. In addition to the gravity and magnetic data, we also used 2D sections taken from the 3D resistivity model to help constrain fault locations in the basin and track low resistivity anomalies throughout the model area. Figure 9 shows the completed profile D which passes through the center of the field site along with a comparison of the fit between the modeled gravity and magnetic response to the observed data and a cross section from the resistivity model which was used to constrain structure at depth.

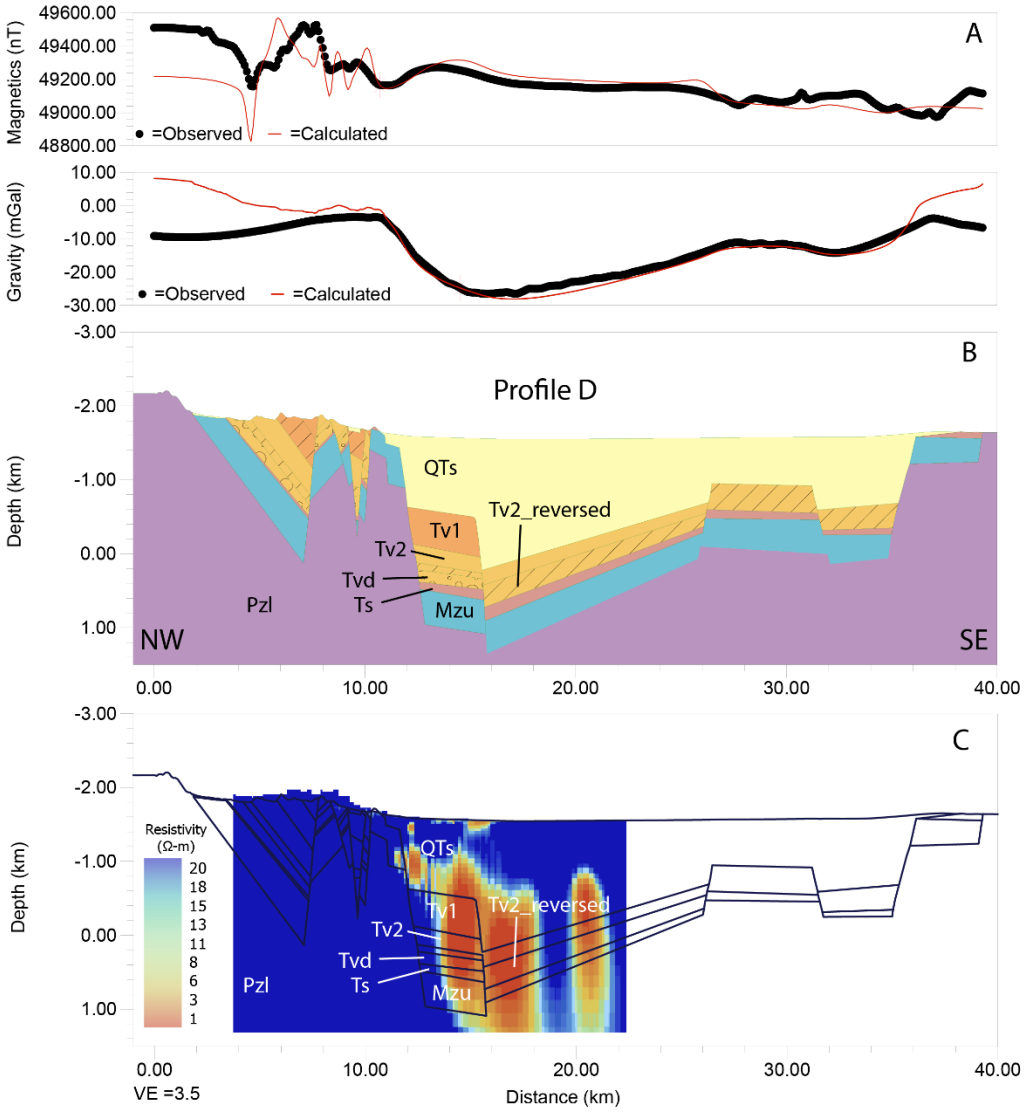

Figure 9: 2D geophysical model of profile D (panel B) along with the modeled gravity and magnetic response compared with the observed data (panel A) and a cross section of the resistivity model superimposed on a wireframe of the model units and inferred structures at depth (panel C).

3.6 3D Geologic Modeling

The implicit 3D modeling software Leapfrog Geo (Seequent, 2025) was used to develop the 3D geologic model of the Lund North site. The model is constructed using the mapped surface contacts of the model units (Figure 8) as well as the subsurface interpretations from the 2D model profiles (e.g., Figure 9). Together these serve as the initial inputs that the program uses to generate 3D surfaces of the geologic contacts throughout the model area. Once the lithology and surface chronologies are properly defined, faults are introduced in a

similar fashion with mapped fault traces containing fault surface expression and 2D profile models defining subsurface fault behavior. Once the program constructs 3D fault surfaces the user must assign a fault chronology/hierarchy wherein fault cross cutting relationships are defined. The software requires that faults either (1) pass through the entire model volume or (2) terminate against faults higher in the user defined, strictly linear fault hierarchy. This can lead to issues with complex fault systems (e.g., at fault terminations, stepovers, etc.) but flexibility in modeling of the non-fault surfaces can help overcome these limitations to produce geologically reasonable models. Once fault systems are activated, the geologic model segments along fault boundaries to allow for modeling of independent fault blocks. Figure 10 shows a 3D perspective view of the preliminary 3D geologic model constructed for the Lund North site.

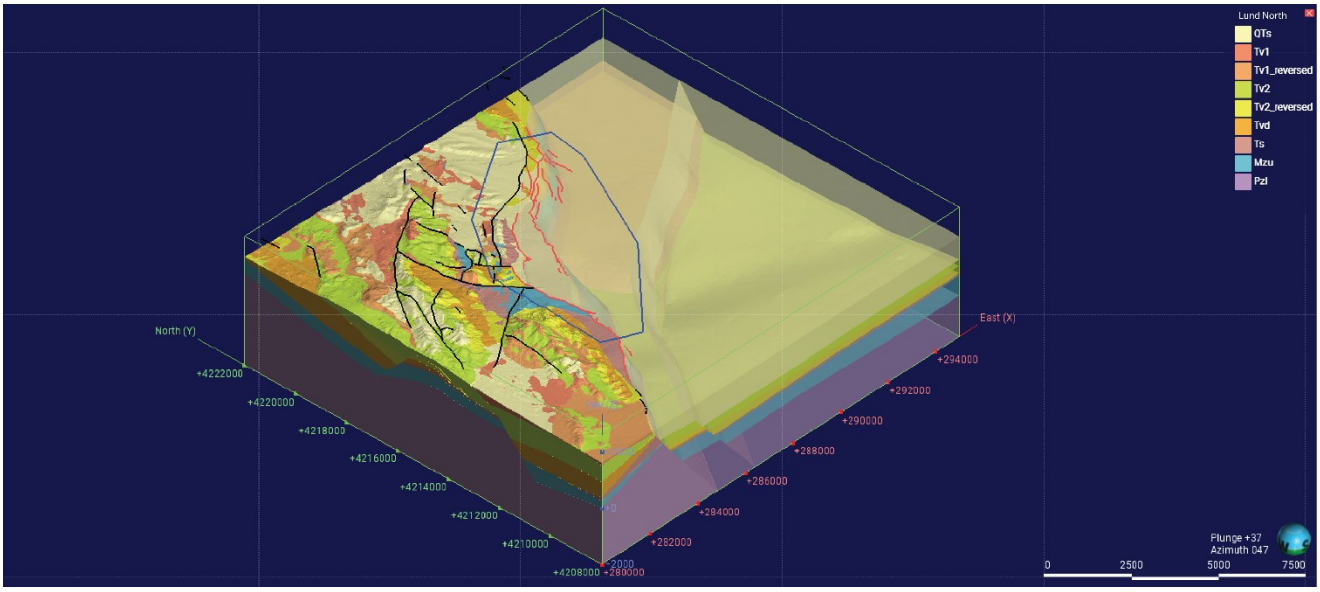

Figure 10: Perspective view of the preliminary 3D geologic model of the Lund North site (looking NE). Active Quaternary faults are shown in red, presumed inactive faults are shown in black. Fault blocks east of the range front are shown with increased transparency to visualize subsurface interpretation. The study area boundary is represented by the blue polygon. Vertical model height is ~3 km.

4. DISCUSSION

The integration of the geophysical techniques and data described above with the surface geology and high-resolution fault mapping in the Lund North area allows for a multifaceted analysis of the geothermal potential of the Lund North site. The gravity and magnetic data augment the fault mapping by providing an independent method for identifying lateral changes in rock properties even when structures are concealed beneath basin fill. Increased structural complexity in a region can enhance permeability and promote geothermal fluid circulation in the subsurface if present, thus making it a useful indicator for geothermal exploration (e.g., Curewitz & Karson, 1997; Faulds & Hinz, 2015). Preliminary structural analysis at Lund North suggested geothermal favorability based on the presence of fault bends and stepovers within the study area boundary (Hardwick et al., 2025). After a more detailed analysis of both the updated Quaternary fault maps and the new geophysical data, we identify two specific areas of structural complexity that could possibly host a geothermal system (Figure 11). The region labeled “A” in figure 11 contains many small fault scarps identified in the lidar data which suggest increased complexity at depth. More importantly, the horizontal gradient lineations from both the gravity and magnetic data at this location are somewhat oblique to the mapped fault traces, suggesting a potential fault bend at depth to a more E-W orientation in the circled area, in contrast to the NE-SW trending surface traces to the north and south. This area is also coincident with the edge of a magnetic high in the basin that we model as a buried volcanic unit. The edge of this unit may be influencing the change in fault orientation at depth and represents an important feature for developing an understanding of the range front fault in this region.

The second area of structural complexity highlighted by the data is seen in the southern portion of the field area labeled “B” in figure 11. The surface trace of the range front fault is mapped as a fault bend, transitioning from a NE-SW strike to approximately N-S. The surface trace continues to follow the topographic boundary to the north, but the gravity gradient data suggest that a second structure continues along a NE-SW strike, possibly linking with a separate NE-SW trending surface trace mapped east of the main topographic range front. Thus, the gravity lineations suggest that there is a fault intersection in this area between the NE-SW trending basin-ward fault and the NE-SW and N-S trending portions of the range front fault. Although unmapped at the surface in the southern portion of the field area, the NE-SW trending structure appears to be the primary feature from a geophysical perspective, and this is consistent with our 2D model profiles which suggest that most of the vertical displacement in the region is accommodated along the basin-ward fault.

In addition to mapping subsurface structure, the magnetic data can also help pinpoint geothermal systems that have contributed to alteration of the surrounding geology. Hydrothermal fluids can alter magnetic minerals (primarily magnetite) in host rock, leading to local magnetic lows that can be used to map out past and/or present geothermal activity. Both regions highlighted in figure 11 contain magnetic lows that could be the result of hydrothermal alteration. The magnetic low seen in area “A” is interpreted here to be associated with

reversely magnetized rocks in the shallow subsurface (Figure 5). Though the presence of reversely magnetized units in area "A" does not preclude the presence of hydrothermal alteration, it does make evaluating its presence less straightforward. In contrast, the more subtle magnetic low seen in Area "B" is more circular in shape (Figure 11 inset), farther from mapped reversed units, and centered over the fault intersection described above. This is more suggestive of local hydrothermal alteration associated with fluids circulating through fault-fractured rock and makes it a target of interest from an alteration perspective.

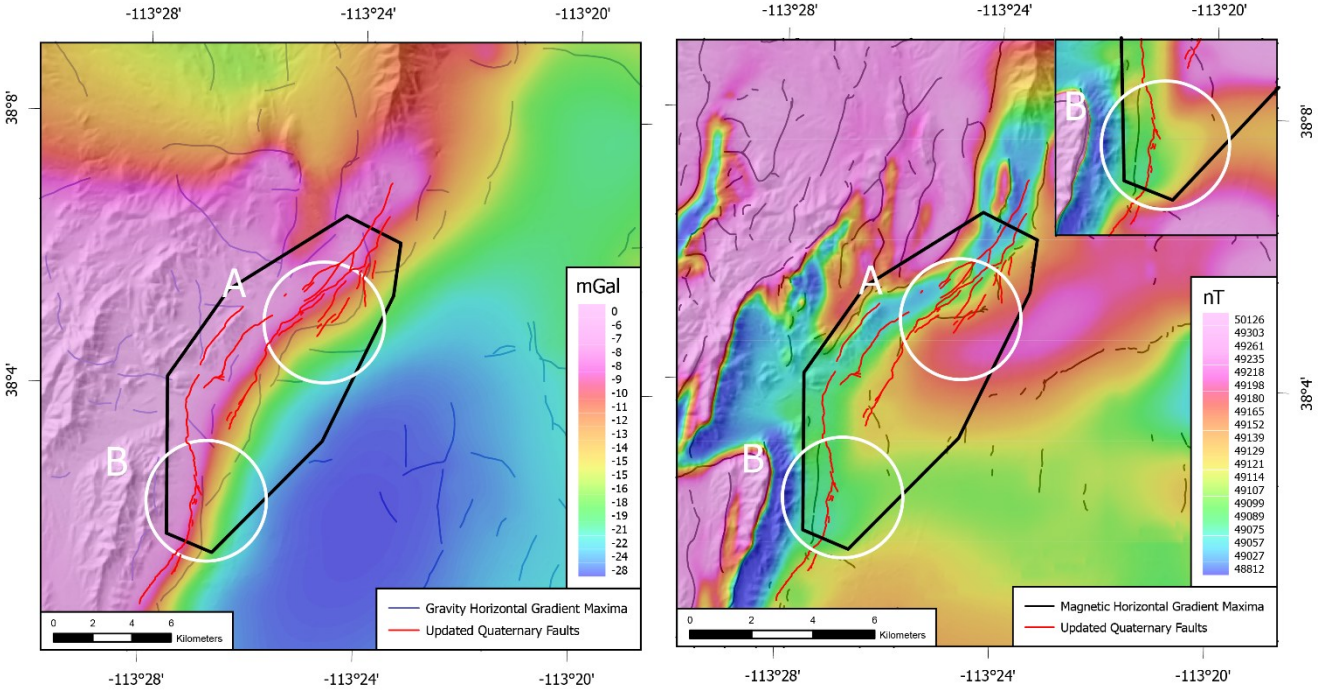

Figure 11: Geophysical maps showing regions of potentially increased structural complexity in the north (A) and south (B) of field area as identified in the isostatic anomaly gravity (left) and reduced-to-pole magnetic (right) data. Inset on right figure shows detailed view of magnetic anomaly in area B. Red lines represent the updated Quaternary fault map. The study boundary is represented by the black polygon. The topographic hillshade was generated from a 30-m DEM taken from the U.S. Geological Survey National Map (U.S. Geological Survey, 2024).

Finally, we can evaluate the relationship between subsurface conductivity and structure by importing isosurfaces from the resistivity model into the 3D geologic model. Figure 12 shows perspective views of the 3D geologic model combined with isosurfaces that represent the most conductive (<30 Ohm-m) portions of the model. There are several shallow conductive bodies that appear to root into deeper, larger bodies at depth suggesting potential fluid flow pathways along the active Quaternary faults. Several of these features sit below the structurally complex region in the north of the field area (Figure 12, panel A) that make them potential candidates for a near-surface geothermal system circulating through fractures associated with the complex faulting in the area. Although there is a similar shallow conductive body near the area of interest in the south (Figure 12, panel B), the conductive anomaly is more isolated and does not appear to link with deeper anomalies which may indicate shallow groundwater rather than a hydrothermal system; however, the magnetic low in this area does suggest some potential for hydrothermal activity.

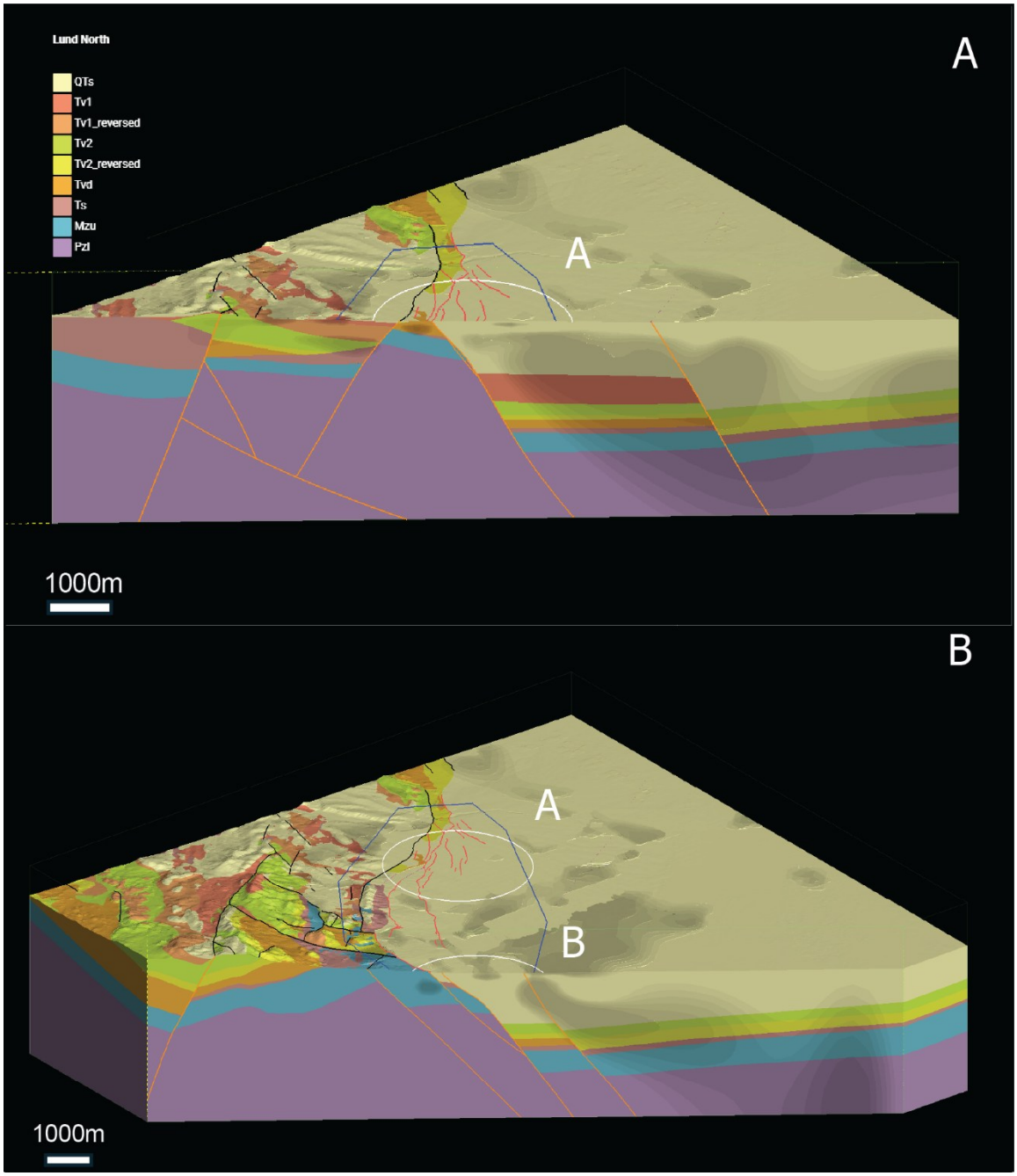

Figure 12: Perspective views of the 3D geologic model combined with <30 Ohm-m isosurfaces taken from the resistivity model (shaded regions). Panel A shows a cross section through the northern region of interest highlighted in figure 11 while panel B shows a cross section through the southern region of interest. Isosurfaces are 30, 25, 20, 15, 10, and 5 Ohm-m from lightest to darkest shaded regions respectively. Active Quaternary faults are shown in red, presumed inactive faults are shown in black. The study area is represented by the blue polygon.

CONCLUSION

The geophysical data collected at Lund North offer key insights into the geothermal potential of the region. When combined with updated structural data and detailed geologic mapping we have developed detailed 2D and 3D models that constrain subsurface geometries of structures and their relationship to conductive anomalies. These models help identify regions of increased structural complexity and can be used in tandem with the 3D resistivity model to indicate which structurally complex zones may host hydrothermal activity. Results suggest at least two sites (A and B above) in the Lund North field area could be potential geothermal systems. Further planned activities include continued refinement of the 3D geologic model so that it can be used in development of a 3D geophysical model that better fits the geophysical data to improve our understanding of the subsurface in these regions of interest. The geophysical data and models will be

combined with additional data collected as a part of the INGENIOUS project (e.g. 2-m temperature and heat flow data), as well as a local-scale play fairway analysis and conceptual model, to select sites for planned thermal gradient hole drilling.

ACKNOWLEDGEMENT

This project is funded by U.S. Department of Energy – Geothermal Technologies Office under award DE-EE0009254 to the University of Nevada, Reno, and with support from the U.S. Geological Survey Energy Resources Program under the Geothermal Resource Investigations project. Any use of trade, firm, or product names is for descriptive purposes only and does not imply endorsement by the U.S. Government. We thank the Milne Family for granting us access to their land for data collection. We thank Callum Walter and Tait Earney for their thoughtful reviews which greatly improved this manuscript. We thank Tait Earney also for his invaluable help with Leapfrog Geo.

REFERENCES

Ayling, B., Faulds, J.E., Clark, A., Morales-Rivera, A., Sladek, C., Berti, C., Kreemer, C., Siler, D., Mlawsky, E., Gentry, E., Kleber, E., Burns, E., Warren, I., Batir, J., DeAngelo, J., Peacock, J., Witter, J., Queen, J., Glen, J.M.G., Kraal, K., Mann, M., Wagoner, N., Williams, N., Dobson, P., Micander, R., Koehler, R., Kirby, S., Brown, S., Earney, T.E., Cladouhos, T., Rickard, B., Trainor-Guitton, W., Lifton, Z. "INnovative Geothermal Exploration through Novel Investigations Of Undiscovered Systems (INGENIOUS) Project Introduction and Activity Update." Proceedings: GRC Transactions, 46, (2022).

Best, M.G., Christiansen, E.H., Deino, A.L., Gromme, S., Hart, G.L., and Tingey, D.G.: The 36–18 Ma Indian Peak–Caliente ignimbrite field and calderas, southeastern Great Basin, USA: Multicyclic super-eruptions. Geosphere; 9 (4), (2013): 864–950. https://doi.org/10.1130/GES00902.1

Blakely, R. J.: Potential theory in gravity and magnetic applications, New York, Cambridge University Press, (1995), 441 p

Blakely, R. J., and Simpson, R. W.: Approximating edges of source bodies from magnetic and gravity anomalies, Geophysics, v. 51, p. 1494–1498, (1986)

Burgess, Q.P., and Faulds., J.E.: Characterization and Analysis of a Potential Hidden Geothermal Resource in the Jersey Summit Area, North-Central, Nevada: Proceedings 49th Workshop on Geothermal Reservoir Engineering, Stanford University, Stanford, CA, SGP-TR-227, (2024), 8 p.

Cronkite-Ratcliff, C., and Athens, N.D., 2025, pymaxspots: Computing and connecting horizontal gradient maxima in potential-field geophysics, U.S. Geological Survey software release, v1.0, https://doi.org/10.5066/P13FSKEM.

Curewitz, D. and Karson, J.A., 1997. Structural settings of hydrothermal outflow: Fracture permeability maintained by fault propagation and interaction: Journal of Volcanology and Geothermal Research, v. 79, no. 3-4, p. 149-168, https://doi.org/10.1016/S0377-0273(97)00027-9.

Day, W.D., 2019, The Earth Mapping Resources Initiative (Earth MRI): Mapping the nations critical mineral resources: U.S. Geological Survey Fact Sheet 2019-3007.

Earney T. E., Glen, J. M., Peacock, J., Faulds, J., Schermerhorn, W., Rea-Downing, G. H., Anderson, J., Lindsey, C., Richards, M., (2024) Geophysical Modeling of a Possible Blind Geothermal System Near Battle Mountain, NV, Geothermal Resource Council Transactions v. 48 p. 1699-1719.

Faulds, J., and Hinz, N.: Favorable tectonic and structural settings of geothermal systems in the Great Basin region, western USA: Proxies for discovering blind geothermal systems, Proceedings World Geothermal Congress, Melbourne, Australia (2015) https://www.osti.gov/biblio/1724082

Faulds, J.E., Hinz, N.H., Coolbaugh, M.F., Ramelli, A., Glen, J.M, Ayling, B.A., Wannamaker, P.E., DeOreo, S.B., Siler, D.L., and Craig, J.W.: Vectoring into potential blind geothermal systems in the Granite Springs Valley area, western Nevada: Application of the play fairway analysis at multiple scales: Proceedings 44th Workshop on Geothermal Reservoir Engineering, Stanford University, Stanford, CA, SGPTR-214, (2019), p. 74-84

Faulds, J.E., Hinz, N.H., Coolbaugh, M., Ayling, B., Glen, J., Craig, J.W., McConville, E., Siler, D., Queen, J., Witter, J. and Hardwick, C.: Discovering blind geothermal systems in the Great Basin region: An integrated geologic and geophysical approach for establishing geothermal play fairways: All phases: Department of Energy, Geothermal Technologies Office, Final Technical Report on Award DE-EE0006731, (2021), 74 p, https://doi.org/10.2172/1724080.

Faulds, J.E., Earney, T.E., Glen, J.M., Queen, J.H., Peacock, J., Hart-Wagoner, N., Kraal, K., Lindsey, C., Burgess, Q., Giddens, M.; Structural setting and geothermal potential of northeastern Reese River Valley, north-central Nevada: Highly prospective detailed study site for the INGENIOUS project, Geothermal Resources Council Transactions, v. 48, (2024), p. 1240-1257.

Gettings, P., Chapman, D.S., and Allis, R.: Techniques, analysis, and noise in a Salt Lake Valley 4D Gravity experiment: Geophysics, v. 73, no. 6, (2008), p. WA71–WA82

Glen, J.M.G., Peacock, J., Earney, T., Schermerhorn, W., Siler, D., Faulds, J.E., and DeAngelo, J. "A Geophysical Characterization of Structure and Geology of the Northern Granite Springs Valley Geothermal System, Northwestern Nevada,." Geothermal Resources Council Transactions, 46, (2022), 20p.,

Hardwick, C. L., Szymanski, E., Hart-Wagoner, N.R., Ashton, S., Christensen, N., Earney, T.E., Faulds, J. E., Glen, J. M., Hiscock, A., Kirby, S., Knudsen, T., Kobe, S., Lindsey, C., Morbeck, B. L., Peacock, J., Rea-Downing, G., Sschermerhorn, W. D., Smith, K. Exploration for Blind Geothermal Systems in the Eastern Great Basin of Utah: An Update on the "Lund North North" INGENIOUS Detailed Study Site. Proceedings, 50th Workshop on Geothermal Reservoir Engineering, Stanford University, Stanford, CA, SGP-TR-229, (2025).

Hart-Wagoner, N., Coolbaugh, M., Faulds, J.E., Mlawsky, E., Lindsey, C., and Trainor-Guitton, W.: Preliminary Regional Play Fairway Workflow for the Great Basin Region, USA. Proceedings, 49th Workshop on Geothermal Reservoir Engineering, Stanford University, Stanford, CA, SGP-TR-227, (2024).

Hildenbrand, T., Briesacher, A., Flanagan, G., Hinze, W., Hittleman, A., Keller, G., Kucks, R., Plouff, D., Roest, W., Seeley, J., Smith, D., and Webring, M. "Rationale and Operational Plan to Upgrade the U.S. Gravity Database." U.S. Geological Survey Open File Report, 02-463, (2002), doi: 10.3133/ofr02463.

Hintze, L.F., Grant, S.K., Weaver, C.L., and Best, M.G., Geologic map of the Blue Mountain-Lund North area, Beaver and Iron Counties, Utah, Miscellaneous Investigation Series Map I-2361. UGS. 1:50,000 scale. (1994) https://doi.org/10.34191/M-156

Hintze, L.F., Grant, S.K., Weaver, C.L., and Best, M.G.: Geologic map of the Blue Mountain - Lund North area, Beaver and Iron Counties, Utah (GIS reproduction of USGS Map I-2361 [1994]: Utah Geological Survey Open-File Report 678DM, 1:50,000 scale, (2017), 1 pl., https://doi.org/10.34191/OFR-678dm.

Jachens, R.C., and Moring, B.C. "Maps of the Thickness of Cenozoic Deposits and the Isostatic Residual Gravity Over Basement for Nevada." U.S. Geological Survey Open File Report, 90-404, (1990), doi: 10.3133/ofr90404.

Jachens, R.C., Moring, B.C., and Schruben P.G. "Thickness of Cenozoic Deposits and the Isostatic Residual Gravity Over Basement" Chapter 2 in Singer, An Analysis of Nevada's Metal-Bearing Mineral Resources, Nevada Bureau of Mines and Geology Open-File Report, 96-02-02, (1996).

Kappler, K., Peacock, J., Egbert, G., Frassetto, A., Heagy, L., Kelbert, A., Keyson, L., Oldenburg, D., Ronan, T., and Sweet, J.: Aurora: An open-source Python implementation of the EMTF package for magnetotelluric data processing using MTH5 and mt_metadata. Journal of Open Source Software. 9. 6832, (2024), 10.21105/joss.06832.

Kelbert, A., Meqbel, N., Egbert, G., and Tandon, K.: ModEM: A modular system for inversion of electromagnetic geophysical data. Computers & Geosciences. 66. (2014), 40-53. 10.1016/j.cageo.2014.01.010.

Peacock, J., Kappler, K., Heagy, L., Ronan, T., Kelberd, A., and Frassetto, A.: MTH5: An archive and exchangeable data format for magnetotelluric time series data, Computers and Geoscience, 162, 105102, (2022)

Schermerhorn, W., and Phelps, G. Airborne magnetic and radiometric survey, west central Utah, 2023-2024. U.S. Geological Survey data release, (2025), https://doi.org/10.5066/P13M9JJT

Seequent, Oasis Montaj, 2024.2, (2024).

Seequent, Leapfrog Geo, 2025.3, (2025).

U.S. Geological Survey, 2020, Quaternary Fault and Fold Database for the Nation, accessed January 18, 2026, at https://doi.org/10.5066/P9BCVRCK

U.S. Geological Survey, 2024, 1 Arc-second Digital Elevation Models (DEMs) - USGS National Map 3DEP Downloadable Data Collection, accessed January 18, 2026 at https://data.usgs.gov/datacatalog/data/USGS:35f9c4d4-b113-4c8d-8691-47c428c29a5b

Utah Geospatial Reference Center (UGRC), 2020, 2020 Central and Southern Utah Lidar Data: https://gis.utah.gov/products/sgid/elevation/lidar/#2020-southern-utah, accessed May 2024. Utah Geological Survey, Utah Geologic Hazards Portal: https://hazards.geology.utah.gov/, accessed December 11, 2024